Solidification Cracking of IN 718 TIG Welds

Myriam Brochu[1,*], Alexis Chiocca[1], Rafael Navalon-Cabanes[1], Jean Fournier[2]

[1] Department of Mechanical Engineering, École Polytechnique de Montréal, Montréal H3T 4A6, Canada
[2] Special Process Development Group, Pratt & Whitney Canada, Longueil J4G 1A1, Canada
* Corresponding author: myriam.brochu@polymtl.ca

Abstract Solidification cracking was observed during a tungsten–inert gas (TIG) welding process used to join two thin sheets of nickel-based superalloy IN718. Microstructural analysis of cracked specimens showed a centerline grain boundary (CLGB) susceptible to limit the hot ductility of the welds. Different welding parameters were modified to avoid the formation of the CLGB; such as the current waveform, the heat input and the welding speed. Results show that it is possible to obtain a microstructure free of a straight CLGB when using a heat input below 135 J/mm. However, to achieve full penetration, the heat input cannot be decreased below 112 J/mm. The experimental results are presented in the form of a weldability map as proposed by Dye et al. and they can be used to predict the range of process parameters favorable to successfully TIG weld IN718 sheet metal.

Keywords Fusion welding, solidification cracking, nickel superalloy, microstructure, process

1. Introduction

1.1. Context

Nickel superalloy IN718 is used to manufacture gas turbine engine components such as disks, cases, shafts, blades, stators, seals, supports, tubes and fasteners [1]. This alloy is selected for its high temperature mechanical properties but also for its weldability, especially its resistance to strain age cracking [2, 3]. Nevertheless, a recurrent weld cracking problem was observed while TIG welding sheets of IN718. Furthermore, in all cracked welds, microstructural observation revealed the existence of a centerline grain boundary. Based on the hypothesis that the CLGB reduces the alloy resistance to solidification cracking [4], the objective of the research project is to identify process conditions that will produce a weld free of CLGB. Our research efforts were oriented toward the improvement of the welding parameters since the weld geometry and the materials chemistry are restricted. To reach our objective, several welding experiments were conducted as reported in section 1. The microstructure of the welds produced was examined and is reported in section 3. In section 4, the effects of the welding speed and of the welding power on the microstructure are discussed. Finally, the practical limitations of the proposed welding conditions are exposed and future work is planned.

1.2. Background: Solidification cracking

Even though alloy 718 is nearly immune to strain age cracking, it is susceptible to other cracking mechanisms such as solidification cracking, heat affected zone liquation cracking, and ductility dip cracking [3]. Solidification cracking happens within the weld, when the deformations induced by the liquid-solid phase transformation and the thermal contraction are higher than the ductility of the mushy zone. This type of cracking occurs more specifically in the last stage of solidification, when the fraction of liquid is less than 10%. The remaining liquid forms a film between the grains and

between dendrites, and the deformations and stresses due to shrinkage of the material grow gradually as solidification is ending, tearing the joint apart.

The amount of minor addition elements such as B, Zr and Nb, have a significant influence on the weldability of nickel alloy IN718. During solidification, segregation of Nb leads to the formation NbC and Lave phases which are widening the solidification range increasing the size of the crack susceptible mushy zone. Moreover, NbC and Lave phases are brittle and deleterious to the weld ductility even after solidification is completed [5].

Since B, Zr and Nb are added intentionally in superalloy IN718 for strengthening purposes, it is important to promote the formation of a homogeneous solidification structure. If the last liquid to be solidified (rich in alloying elements) is concentrated in one region, the weld ductility can be reduced significantly [6, 7]. This is the case when a centerline grain boundary (CLGB) forms. Weld microstructures with a CLGB are susceptible to crack propagation along the length of the weld just behind the melt. Welding can be successful (no cracking) for welds having a CLGB. However, the unevenly distributed fragile phases will create a weak plane that can compromise the weld mechanical properties [8]. For these reasons, a straight centerline grain boundary is an unwanted feature often related to solidification cracking [4].

2. Methodology

2.1. Nominal welding conditions and microstructure

The TIG welds for which cracking occurred are but-welded IN718 sheet rings having an average thickness of 1.33 mm. The nominal chemical composition of the sheet material and the nominal welding parameters are reported in Table 1 and 2 respectively.

Table 1. Chemical composition of nickel superalloy IN718 (weight %)[1,2]

	Ni	Cr	Nb	Mo	Ti	Al	Co	Mn	Si	Cu	Ta	C	B
Min.	50.00	17.00	4.75	2.80	0.65	0.20							
Max.	55.00	21.00	5.50	3.30	1.15	0.80	1.00	0.35	0.35	0.30	0.05	0.08	0.006

[1]Remaining is iron [2] Phosphorus and sulfur content must be below 0.015

Table 2. Welding parameters

DC Current I (A)	Voltage U (V)	Welding Speed WS (mm/s)	Filler wire speed (mm/s)	Diameter of filler wire (mm)	Electrode angle (^{o})	Linear Heat input HI (J/mm)[1]
86	8	5.27	5.72	0.889	45	140

[1]Calculated by $\boldsymbol{HI = \frac{U*I}{WS}}$

Visual and optical microscopy observations were performed on cracked specimens to identify the failure mechanism. The longitudinal aspect of the crack, its position at the center of the fusion zone, and its interdendritic path led to the identification of a solidification cracking problem. The same features were observed by Kerrouault [9] and Shinozaki et al. [10] while monitoring solidification cracking in austenitic stainless steels. Moreover, the microstructure of all specimens observed contained a centerline grain boundary (CLGB) as shown in Fig. 1.

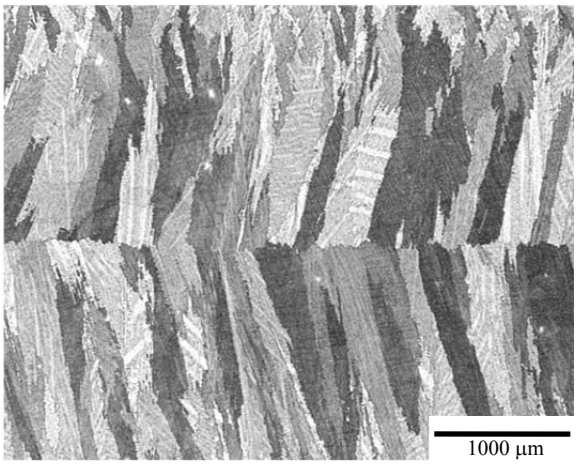

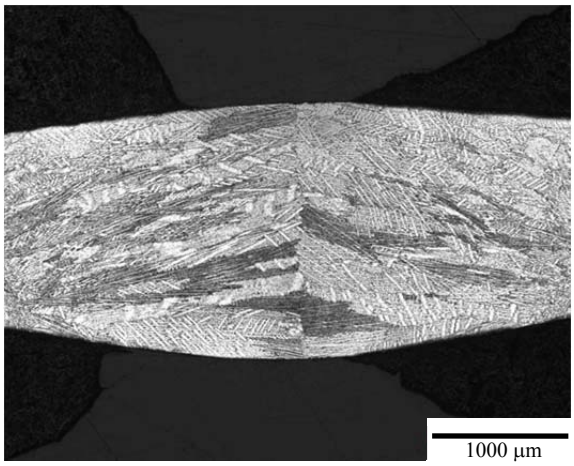

a) Longitudinal section b) Cross section

Figure 1. Typical microstructure of a cracked specimen revealed with etchant composed of 5% H_20_2 (30%), 47.5% HCl (40%) and 47.5% methanol

2.2 Welding experiments

Experiments were performed to identify a range of welding parameters that creates a weld free of CLGB. The ideal microstructure would be fully or partly equiaxe and fine. If it is impossible to form equiaxe grains, a more tortuous central grain boundary would be an improvement of the actual microstructure. To reach the objective, theoretical considerations were reviewed and the following approaches were tested:

2.2.1 Current pulsing,

2.2.2 Constitutional supercooling,

2.2.3 Weld pool shape control.

Tests were done on rectangular sheet coupons having a thickness of 1.27 mm. Two coupons were firmly clamped together and a semi-automated TIG machine was used to produce a straight 10 cm long weld. Longitudinal and cross sections of the welds were prepared for metallographic observations.

2.2.1. Current pulsing

According to the results of Ram and Reddy [8], current pulsing can produce a weld with a fine and homogeneous microstructure which considerably improve the weld ductility at 650°C. Their study was performed for autogeneous welding of 2 mm thick sheets of IN718. In another paper from the same research team, it was explained that current pulsing increases the cooling rate resulting in significant refinement of the fusion zone structure [11].

In our study, current pulsation was attempted at a frequency of 3.3 hertz using four different current ratios (low current/high current) as reported in Table 3. The welding speed and the filler wire speed were kept constant at values of 3.39 mm/s and 4.66 mm/s respectively. This welding speed is lower than the nominal welding speed for which the cracking problem was initially observed. It was decided to reduce the welding speed following unsuccessful current pulsation welding tests

performed at a welding speed of 5.2 mm/s. In the experiments of Sivaprasad et al. [11] the beneficial effect of current pulsation was observed for a welding speed of 1.11 mm/s. Overall, 4 specimens were welded (Pulse 1 to 4 in Table 3) and the fusion zone microstructure was observed as will be presented in section 3.1.

Table 3. Welding parameters for the current pulsing experiments

		Pulse 1	**Pulse 2**	**Pulse 3**	**Pulse 4**
Voltage, U (V)		8.0	8.0	8.0	8.0
Current parameters	Current ratio	0.66	0.42	0.35	0.21
	Low Current, LC (A)	54.0	40.0	30.0	20.0
	Low time, LT (s)	0.15	0.15	0.15	0.15
	High Current, HC (A)	82.0	96.0	86.0	96.0
	High time, HT (s)	0.15	0.15	0.15	0.15
Welding speed, WS (mm/s)		3.39	3.39	3.39	3.39
Filler wire speed (mm/s)		4.66	4.66	4.66	4.66
Heat Input[1], HI (J/mm)		160.6	160.6	137.0	137.0
Welding Power[2], W (Watt)		544	544	464	464

[1]Calculated by $\mathbf{HI} = \frac{\mathbf{U}*(\mathbf{LC}*\mathbf{LT}+\mathbf{HC}*\mathbf{HT})}{(\mathbf{LT}+\mathbf{HT})*\mathbf{WS}}$ [2] Calculated by $\mathbf{W} = \frac{\mathbf{U}*(\mathbf{LC}*\mathbf{LT}+\mathbf{HC}*\mathbf{HT})}{(\mathbf{LT}+\mathbf{HT})}$

2.2.2. Constitutional supercooling

Theoretically, equiaxe grains can form spontaneously in supercooling conditions. This should be achieved by welding in conditions of high solidification rate (R) but low temperature gradient (G) as proposed by Kou et al. [12]. To produce such conditions within the weld pool, the welding speed and the welding power were increased as presented in Table 4. Three trials (SC1 to SC3) were conducted at a high welding speed (8.47 mm/s) and with an increasing welding power as reported in Table 4. The filler wire speed was also increased in order to reproduce comparable weld geometries. According to the theoretical solidification map of Gaümann et al. [13] obtained for nickel superalloy CMSX-4, these welding conditions should result in the formation of equiaxe dendrites. The resulting microstructures will be presented in section 3.2.

Table 4. Welding parameters for constitutional supercooling

	SC 1	**SC 2**	**SC 3**
Voltage, U (V)	7.8	7.8	7.8
Current (A)	121.9	137.5	147.5
Welding speed, WS (mm/s)	8.47	8.47	8.47
Filler wire speed (mm/s)	9.53	9.53	9.53
Heat Input[1], HI (J/mm)	112.2	124.0	135.8
Welding power[2], W (Watt)	951	1072	1150

[1]Calculated by $\mathbf{HI} = \frac{\mathbf{U}*\mathbf{A}}{\mathbf{WS}}$ [2] Calculated by W = U*A

2.2.3. Weld pool shape control

According to the work of Savage [14] an elliptical weld pool shape promotes the formation of a microstructure composed of columnar dendrites but free of CLGB. CLGB forms when columnar grains growing perpendicular to the solid walls meet at the center of the weld. This type of microstructure is typically observed at high welding speed when a tear drop shape weld pool forms. Welding conditions can be modified to favor grain curvature and avoid the formation of a CLGB. Reducing the welding speed favors the formation of an elliptical weld pool and the curvature of grains within the longitudinal plane as experimented by Kou and Le [12]. Moreover, reducing the heat input reduces the depth to width ratio of a weld which favors the formation of a radial grain structure [3] which is also beneficial to the microstructure. It was attempted to produce a weld with an elliptical pool shape and with a low depth to with ratio by decreasing the weld speed (WS) and the heat input (HI) as proposed in Table 5. The filler wire speed was also decreased in order to reproduce comparable weld geometries. Overall, 5 specimens were welded (a combination of 3 WS and 3 HI) and their microstructures were observed as will be presented in section 3.3.

Table 5. Welding parameters for the elliptical weld

	WS 1, HI 1	**WS 1, HI 2**	**WS 1, HI 3**	**WS 2, HI 1**	**WS 3, HI 1**
Voltage, U (V)	8.0	8.0	8.0	8.0	8.0
Current (A)	94.0	85.0	74.0	60.0	44.6
Welding speed (mm/s)	5.27	5.27	5.27	3.39	2.54
Filler wire speed (mm/s)	5.72	5.72	5.72	4.66	2.79
Heat Input[1] (J/mm)	142.7	129.0	112.3	141.6	140.5
Welding power[2], W (Watt)	752	544	592	480	357

[1]Calculated by $\mathbf{HI} = \frac{\mathbf{U*A}}{\mathbf{WS}}$ [2] Calculated by W = U*A

3. Results

3.1. Current pulsing

All welds produced with pulsed current have a similar microstructure which is shown in Fig. 2. Current pulsing did not have the expected effect on the microstructure and changing the current ratio had no significant influence. The most noticeable feature observed by comparing Fig. 2 to Fig. 1, is the existence of a longitudinal grain at the centerline of the welds produced with pulsed current. This was possibly caused by the reduction in welding speed rather than by the current pulsing as will be shown in section 3.3. The formation of a longitudinal grain is not beneficial to the weld microstructure. The grain is coarse and it is bounded by two weak planes oriented perpendicularly to the transversal stresses.

According to the work of Sivaprasad and al. [11], current pulsing is more effective for welds performed at low heat input. Their experiments were done on 3 mm thick sheets at a heat input of 180 J/mm. The experiments presented in this document were performed on 1.2 mm thick sheets using a heat input as low as 137.0 J/mm. The heat input range is comparable considering that our

weld thickness is about 2 mm when considering the addition of the filler material.

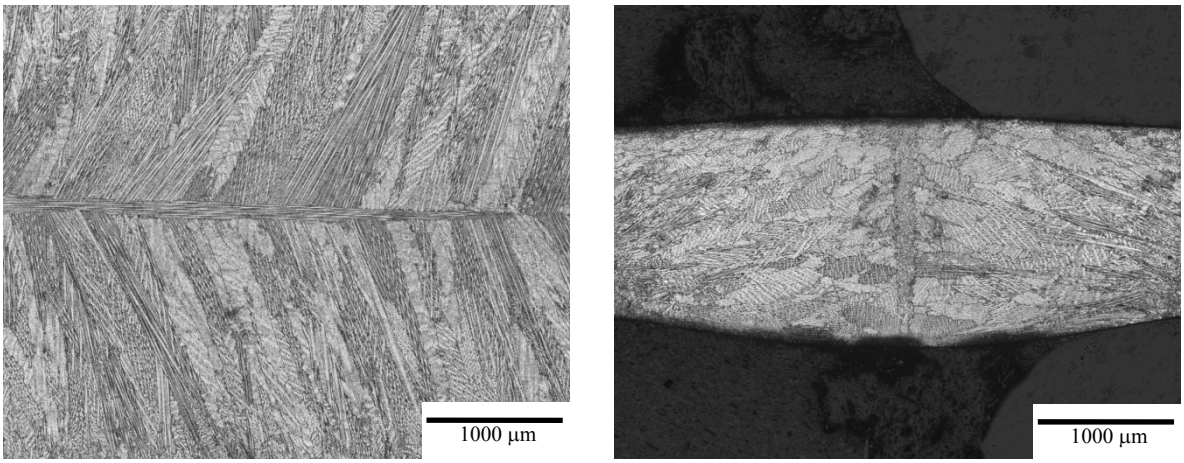

a) Longitudinal section b) Cross section

Figure 2. Typical microstructure of the specimens welded with pulsed current, welding speed of 3.39 mm/s (Pulse 1)

3.2. Supercooling

Within the conditions tested to produce equiaxe dendrites in supercooling conditions, the microstructure obtained with the highest welding power (SC3) is presented in Fig. 3. On Fig.3a showing a top view of the weld, it is clear that the centerline is not as marked as on Fig. 1. However, few equiaxe and fine dendritic grains were formed. Four grains having an equiaxe shape are circled on Fig. 3a. On the cross section of the weld, it is more difficult to evaluate the grain geometry because of the orientation of the cutting plane. If columnar grains are cut on a plane that is not parallel to the grains, it could look equiaxe. Nevertheless, from Fig 3b it can be noticed that the centerline junction is more tortuous than in Fig. 1. This should have a beneficial effect on the resistance to hot cracking and on the mechanical properties of the weld. The microstructures of the welds produced in the two other "supercooling conditions" are comparable to Fig. 3 but with less equiaxe grains. This is an indication that further increasing the speed and the welding power could lead to the desired microstructure.

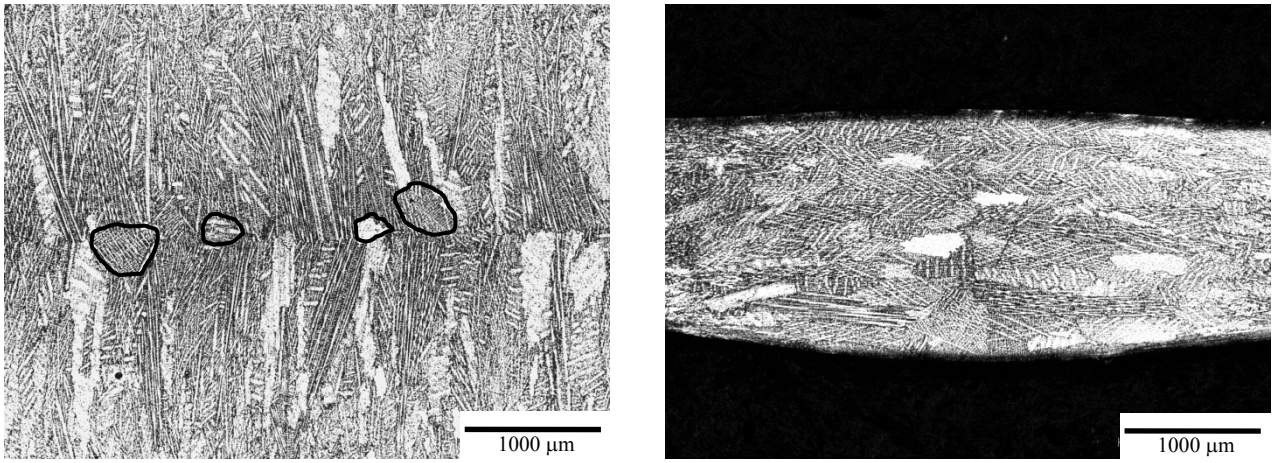

a) Longitudinal section b) Cross section

Figure 3. Microstructure of the weld performed at a welding speed of 8.47 mm/s and with the highest welding power (SC3)

3.3. Weld pool shape

The pictures reported on Fig. 4 show that it was possible to obtain an elliptical pool shape by a reduction of the welding speed. However, the reduction of the welding speed did not cause a significant grain curvature as shown on Fig. 5a. On the other hand, a longitudinal grain formed at the center of the weld. At the lowest welding speed (2.54 mm/s), a thicker longitudinal grain was observed and there was still no evidence of grain curvature.

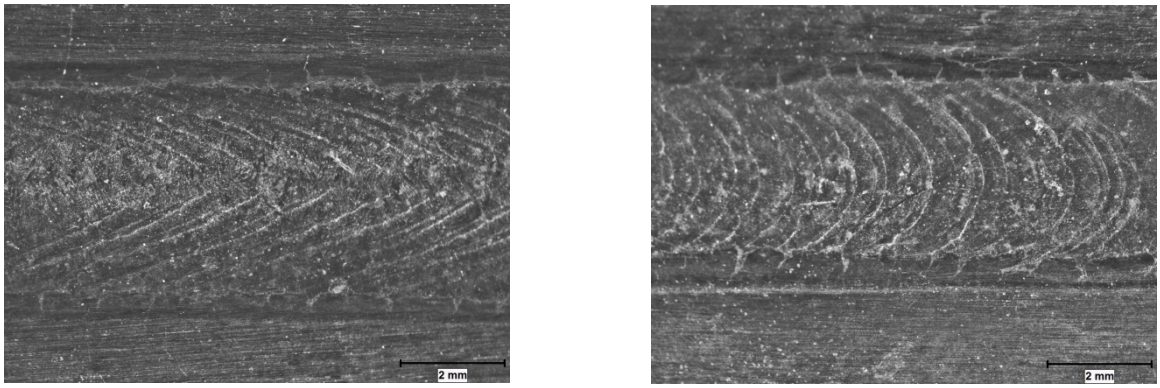

a) Welding speed of 5.27 mm/sec (WS 1, HI 1) b) Welding speed of 2.54 mm/sec (WS 3, HI 1)

Figure 4. Weld pool shape at two different speed, for the same heat input (142 J/mm)

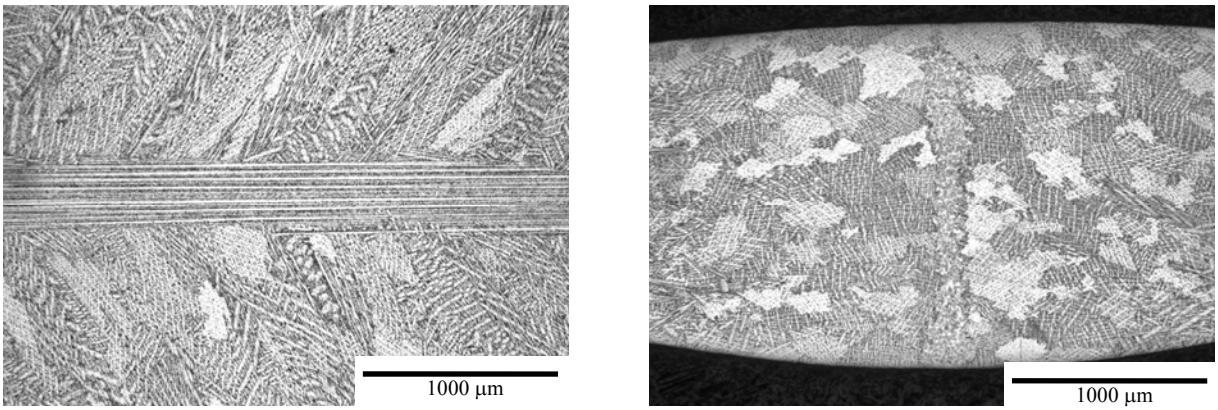

a) Longitudinal section b) Cross section

Figure 5. Microstructure of the specimen produced at 3.39 mm/sec (WS 2, HI 1)

The effect of a reduction in heat input is shown on Fig. 6. The microstructure observed was produced at the same speed as the ones shown in Fig. 1 (5.27 mm/s) but at a heat input of 129.0 J/mm rather than 140.0 J/mm. Reducing the heat input had the expected effect on grain growth. The grain growing direction tilted toward the top of the weld (radial grain growth). This is beneficial to the weld microstructure as it avoids the formation of a sharp centerline. On Fig. 6a and b, the grains nearly seem equiaxe but this could be an optical illusion caused by the fact that the growing directions of the grain are not parallel to the cross section and the longitudinal plane. To produce radial grain growth, it is necessary to promote the formation of a V shape weld. Such a weld is however more susceptible to incomplete penetration. In fact, the weld produced at a heat input of 112.3 J/mm was not fully penetrated.

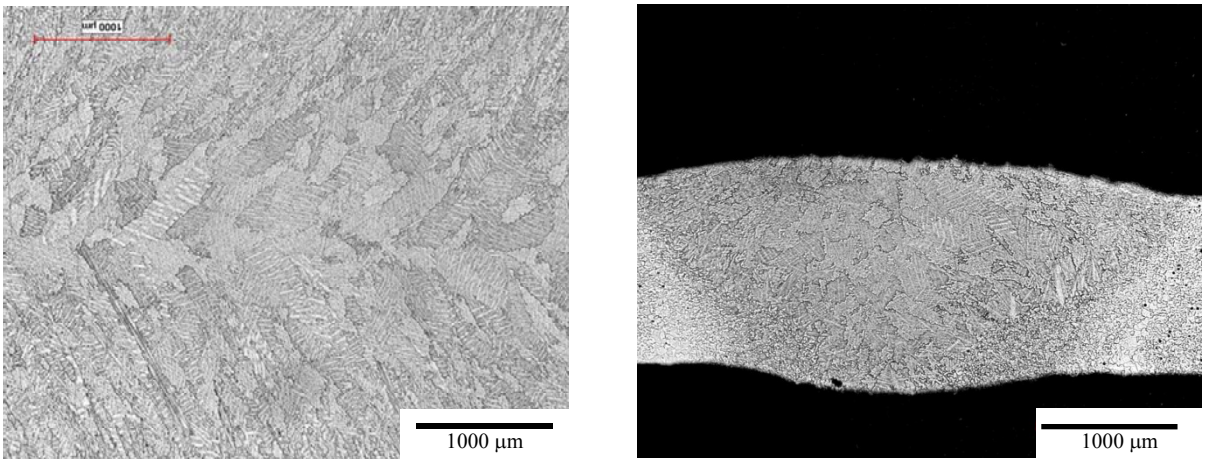

a) Longitudinal section b) Cross section

Figure 6. Typical microstructure of the weld produced at 129 J/mm and 5.27 mm/s(WS 1, HI 2)

4. Discussion

To analyze the microstructural observations, all the test conditions described in section 3 were reported in a graph of the effective welding power (efficiency × current × voltage) versus the welding speed (Fig. 7a). Such a graph was used by Dye et al. to study the effect of the welding parameters on the microstructure of autogeneous TIG welds in IN718 [15]. For the purpose of result presentation, we used a power efficiency factor of 75% as proposed by Dye et al. In Fig. 7a, the microstructural features of the welds are represented by different symbols. Empty circles indicate that the weld is not fully penetrated. Welds without a straight centerline grain boundary, such as the ones shown in Fig. 3 and 6, are presented by full circles. Welds showing a straight centerline grain boundary (CLGB) are presented by full rectangles. Finally, welds with a longitudinal grain (LG) are reported using empty rectangles. To complete the map, we performed additional tests at different welding speed and welding power. In the map of Fig. 7a, the "weldable area" is defined by combinations of welding speed and welding power leading to a fully penetrated weld, free of CLGB and of LG. The "weldable area" was circumscribe using three straight lines. Two lines of constant heat input represented the frontier for the formation of a centerline grain boundary (HI = 134 J/mm) and for incomplete penetration (HI = 112 J/mm). The boundary for the formation of a longitudinal grain was fixed to a constant weld speed of 3.39 mm/sec (vertical line). According to these boundaries, the weldability area identified is very narrow.

Dye et al. predicted theoretically a weldabilty diagram for the autogeneous TIG welding of 2 mm thick IN718 sheets. In Fig. 7b, we adapted their predictions to our sheet thickness. To fit our experimental results at a welding speed of 4.23 mm/sec, the ratio $\Delta x/\rho$ characterizing the CLGB criterion was adjusted to 0.75. Other material and process related constants were considered identical to Dye et al. A comparison of our experimental map (Fig.7a) with the theoretical map of Dye et al., reveals three significant observations. First, the incomplete penetration criterion of Dye et al. is adapted to our weld configuration. Secondly, the criterion proposed for the formation of a centerline grain boundary is not well adapted. According to Dye et al., as the welding speed decreases, a microstructure free of centerline grain boundary could be obtained for a wider range of

welding power. Our results are following an opposite trend. Our experimental criterion for the formation of a CLGB is nearly parallel to the incomplete penetration criterion. The third and final observation concerns the weld speed. In all welds done at a welding speed below 3.39 mm/s, a longitudinal grain formed. This weld microstructure was not reported by Dye et al. and is not acceptable for our application. A lower speed limit criterion was thus added to the map of Fig. 7a.

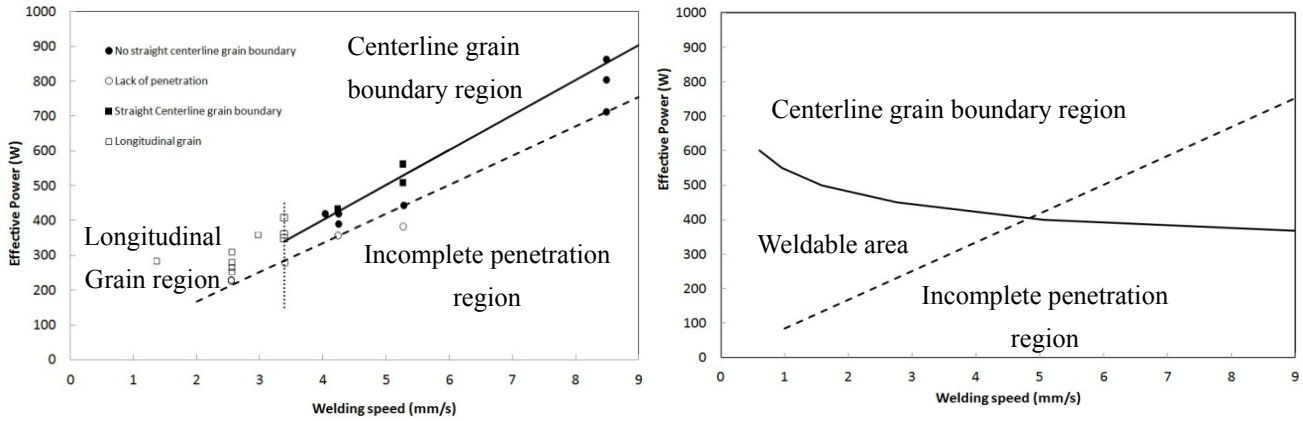

a) Experimental b) Predicted by Dye et al. model

Figure 7. Weldability map

5. Conclusion

The TIG weldability of IN718 sheets was studied in order to reduce the occurrence of solidification cracking. The objective of the experimental work was to identify welding parameters that would prevent the formation of a centerline grain boundary within the weld microstructure. Three welding strategies were tested and the results are summarized below:

Current pulsation

Current pulsation did not improve our weld microstructure and modifying the current ratio had no significant effect on the weld microstructure.

Constitutional supercooling

Welding at high speed and power did not produce the expected fine and equiaxe microstructure. However, the formation of few equiaxe grains suggests that nucleation of grains from the weld pool could happen.

Weld pool shape control

By controlling the depth to width ratio, an improvement of the microstructure was observed. Grain growth inclination resulted in a microstructure free of centerline grain boundary, but partially penetrated welds were produced at heat input below 112 J/mm. Decreasing the welding speed had a detrimental effect since a longitudinal grain formed within the welds performed at welding speed below 3.39 mm/s.

Results reported in a weldability diagram revealed that the weldable area of our IN718 TIG weld is very narrow, for the range of welding conditions tested. This is caused by the fact that the centerline grain boundary criterion is nearly parallel and very close to the incomplete penetration criterion. In practice, restricting the welding power in such a narrow band is limiting. Adjustments of the current intensity are often necessary to better control the dimensions of the assembly and the penetration of

the welds. Further studies should be done in order to identify other welding conditions susceptible to produce a metallurgically sound weld. According to our results, the supercooling strategy should be investigated further. Usage of a current pulsation or cooling shielding gas could favor the germination of equiaxe dendrites in the weld pool.

Acknowledgements

The authors wish to acknowledge Pratt & Whitney Canada for their support.

References

[1] D. F. Paulonis and J. J. Schirra, "Alloy 718 at Pratt and Whitney - Historical perspective and future challenges," in *Superalloys 718, 625, 706 and Various Derivatives, Jun 17 - 20 2001*, Pittsburgh, PA, United states, 2001, pp. 13-23.
[2] B. T. Alexandrov, J. C. Lippold, and N. E. Nissley, "Evaluation of Weld Solidification Cracking in Ni-Base Superalloys Using the Cast Pin Tear Test," in Th. Böllinghaus, H. Herold, C.E. Cross, C. Lippold (Eds.), Hot Cracking Phenomena in Welds II, Berlin, 2008, pp. 193-213.
[3] J. N. Dupont, J. C. Lippold, and S. D. Kiser, Welding metallurgy and weldability of nickel-base alloys, Hoboken, New Jersey: John Wiley & Sons, 2009.
[4] O. Hunziker, D. Dye, and R. C. Reed, "On the formation of a centreline grain boundary during fusion welding," *Acta Mater,* vol. 48, pp. 4191-4201, 2000.
[5] G. Sjoberg, T. Antonsson, S. Azadian, R. Warren, and H. Fredriksson, "Effect of -phase on the weldability and the hot ductility of alloy 718," in *6th International Symposium on Superalloys 718, 625, 706 and Derivatives, October 2, 2005 - October 5, 2005*, Pittsburgh, PA, United states, 2005, pp. 351-362.
[6] W. F. Savage and B. M. Krantz, "Investigation of hot cracking in hastelloy X," *Welding J,* vol. 44, pp. 13--25, 1966.
[7] G. D. J. Ram, A. V. Reddy, K. P. Rao, and G. M. Reddy, "Control of Laves phase in Inconel 718 GTA welds with current pulsing," *Sci Technol Weld Joi,* vol. 9, pp. 390-398, 2004.
[8] G. D. Janaki Ram, A. V. Reddy, K. P. Rao, and G. M. Reddy, "Improvement in stress rupture properties of inconel 718 gas tungsten arc welds using current pulsing," in *J Mater Sci*, 2005, pp. 1497-1500.
[9] N. Kerrouault, "Fissuration à chaud en soudage d'un acier inoxydable austénitique," Ph.D. Ph.D., Mécanique et Matériaux, Ecole Centrale des Arts et Manufactures, Châtenay-Malabry Cedex, 2000.
[10] K. Shinozaki, Y. Motomichi, P. Wen, and T. Tomoko, "Prediction of occurrence of solidification cracking in weld metal," *Weld Inter,* vol. 24, pp. 942-8, 2010.
[11] K. Sivaprasad, S. Ganesh Sundara Raman, P. Mastanaiah, and G. Madhusudhan Reddy, "Influence of magnetic arc oscillation and current pulsing on microstructure and high temperature tensile strength of alloy 718 TIG weldments," *Mat Sci Eng A,* vol. 428, pp. 327-331, 2006.
[12] S. Kou and Y. Le, "Welding parameters and the grain strudture of weld metal - A thermodynamic consideration," *Metall Trans A, Physical metallurgy and materials science,* vol. 19 A, pp. 1075-1082, 1988.
[13] M. Gaumann, C. Bezencon, P. Canalis, and W. Kurz, "Single-crystal laser deposition of superalloys: processing-microstructure maps," *Acta Mater,* vol. 49, pp. 1051-62, 2001.
[14] W. F. Savage, "1980 Houdremont lecture - Solidification, segregation and weld imperfections," *Welding in the World, Le Soudage Dans Le Monde,* vol. 18, pp. 89-114, 1980.
[15] D. Dye, O. Hunziker, and R. C. Reed, "Numerical analysis of the weldability of superalloys," *Acta Mater,* vol. 49, pp. 683-697, 2001.